Received: 14 March 2022 | Revised: 10 June 2022 | Accepted: 3 August 2022

DOI: 10.1002/jcc.26986

RESEARCH ARTICLE

Journal of COMPUTATIONAL CHEMISTRY WILEY

Zinc oxide nanoclusters and their potential application as CH_4 and CO_2 gas sensors: Insight from DFT and TD-DFT

İskender Muz[1] | Mustafa Kurban[2]

[1]Department of Mathematics and Science Education, Nevşehir Hacı Bektaş Veli University, Nevşehir, Turkey

[2]Department of Electrical and Electronics Engineering, Kırşehir Ahi Evran University, Kırşehir, Turkey

Correspondence
İskender Muz, Department of Mathematics and Science Education, Nevşehir Hacı Bektaş Veli University, 50300 Nevşehir, Turkey.
Email: iskendermuz@yahoo.com

Mustafa Kurban, Department of Electrical and Electronics Engineering, Kırşehir Ahi Evran University, 40100 Kırşehir, Turkey.
Email: mkurbanphys@gmail.com

Abstract

We have investigated the adsorption of CH_4 and CO_2 gases on zinc oxide nanoclusters (ZnO NCs) using density functional theory (DFT). It was found that the CH_4 tends to be physically adsorbed on the surface of all the ZnO NCs with adsorption energy in the range −11 to −14 kcal/mol. Even though, the CO_2 is favorably chemisorbed on the $Zn_{12}O_{12}$ and $Zn_{15}O_{15}$ NCs, with adsorption energy about −38 kcal/mol at B3LYP/6-311G(d,p) level of theory. When the CH_4 and CO_2 gases are adsorbed on the ZnO NCs, their electrical conductivities are decreased, and thus the studied ZnO NCs do not generate an electrical signal in the presence of CH_4 and CO_2 gases. Interestingly, both pure and gas adsorbed $Zn_{22}O_{22}$ NC exhibited more favorable electronic and reactive properties than other NCs. Comparison of the structural, electronic, and optical data predicted by DFT/B3LYP and TD-DFT/CAM-B3LYP calculations with those experimentally obtained show good agreement.

KEYWORDS
adsorption, DFT, electrical conductivity, gas sensors, zinc oxides

1 | INTRODUCTION

Over the last decades, human modernization activities such as burning fossil fuels and rapid industrial revolution have given rise to an increase in the emission of greenhouse gases, most importantly, CO_2 and CH_4 in the atmosphere and thus trigger global warming, and climate change. In this context, many efforts have been carried out using nanomaterials to store or capture CO_2 and CH_4 and efficiently mitigate the concentration of greenhouse gases.[1–6] Among nanomaterials, different forms of ZnO nanostructures such as nanoparticles, nanowires, nanotubes, and so forth have been of great interest in many areas including solar cells, the light-emitting/detecting diodes, gas sensors, and so forth.[7–16] ZnO nanoparticles (NPs)/quantum dots (QDs), more specifically, have been significant attention because of their desirable features such as strong adsorption capability and easily tunable surface making them possible to use in important areas such as photosensors[17] and electronics.[18]

The adsorption process is very simple, economical, effective with easy regeneration, and thus provides a promising alternative[19] to reduce the increasing CO_2 and CH_4 emissions in the environment. In the literature, for example, porous oxide materials have been recognized as promising candidates for CO_2 capture.[20] Many oxide materials including MgO and CaO are extensively studied as CO_2 adsorbents. ZnO which is among the most used metal oxide due to its desirable properties has been investigated little in this aspect.

This research investigates the role of ZnO nanoclusters (NCs) with different sizes as CO_2 and CH_4 capture material. First, all possible initial orientations of the CO_2 and CH_4 were studied on the surface of the ZnO NCs. Then the stability was determined based on the structures with the lowest total energies. The structural parameters, the point group, dipole moment, binding energy, HOMO–LUMO energy gap, the density of state, vertical ionization potential, vertical electron affinity, hardness, chemical potential, and electrophilic index of all the NCs were also calculated. The UV–vis absorption spectra for CH_4 and CO_2 adsorptions on the surface of ZnO NCs also calculated using TD-DFT method. Finally, the effect of the size of ZnO on the adsorption of CO_2 and CH_4 has been discussed in detail.

2 | COMPUTATIONAL DETAILS

The adsorption configurations of CH_4 and CO_2 gases on the $Zn_{12}O_{12}$, $Zn_{15}O_{15}$, $Zn_{18}O_{18}$, $Zn_{20}O_{20}$, $Zn_{22}O_{22}$, and $Zn_{24}O_{24}$ nanoclusters (NCs) were evaluated under the framework of DFT calculations using the B3LYP functional and 6-311G(d,p) level[21] with the Gaussian 09 software.[22] Subsequently, frequency analysis calculations were also performed at the same level of theory to confirm that the geometries are a true minimum. All the configurations were modeled by varying the orientation of ZnO NCs with respect to CH_4 and CO_2 gases (see Figure 1) and by considering reactive sites of complexes through the molecular electrostatic potential (ESP) which is plotted by VMD program.[23]

To deeply understand the electronic properties of complexes, the DOS for the each absorbed gas were carried out by using GaussSum program.[24] In addition, the adsorption energies (E_{ad}) of gases on ZnO NCs were calculated by following equation:

$$E_{ad} = E\left(\frac{\text{Gas}}{\text{ZnO}}\right) - E(\text{ZnO}) - E(\text{Gas}), \quad (1)$$

where, $E\left(\frac{\text{Gas}}{\text{ZnO}}\right)$ is the total energy of the gas adsorbed upon pure ZnO NCs, $E(\text{ZnO})$ and $E(\text{Gas})$ are the total energies of isolated adsorbate Gas and ZnO NCs, respectively.

For the CH_4 and CO_2 gases adsorbed upon ZnO NCs, the quantum molecular descriptors[25] chemical hardness (η), chemical potential (μ) and electrophilicity index (ω) were determined from Koopman's theorem[26] using HOMO and LUMO energies as following: $\eta = (I - A)/2$ and $\omega = \mu^2/2\eta$. VIP and VEA were evaluated using the following relationships: $[\text{VIP} = E^{\text{cation}} - E^{\text{neutral}}]$ and $[\text{VEA} = E^{\text{neutral}} - E^{\text{anion}}]$. These parameters are important to gain insight into ionization and electron attachment, respectively, based on the comparative calculation of anion and cation optimized structures with neutral geometry. In addition, time-dependent DFT (TD-DFT) calculations based on CAM-B3LYP functional[27] with 6-311G(d,p) basis set is applied for guessing UV–vis spectra. It should also be noted that the CAM-B3LYP functional is better than the B3LYP when it comes to excited state energies.[28–31] Hence, one way to remedy this is to calculate

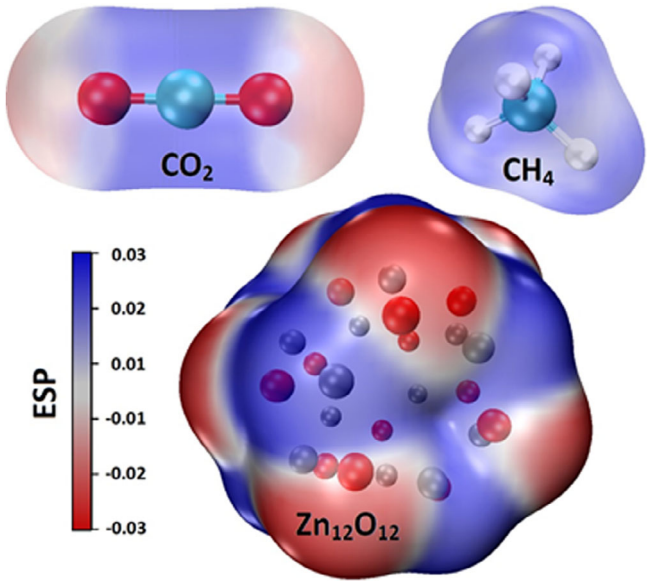

FIGURE 1 The molecular electrostatic potential (ESP) patterns of CO_2, CH_4, and $Zn_{12}O_{12}$

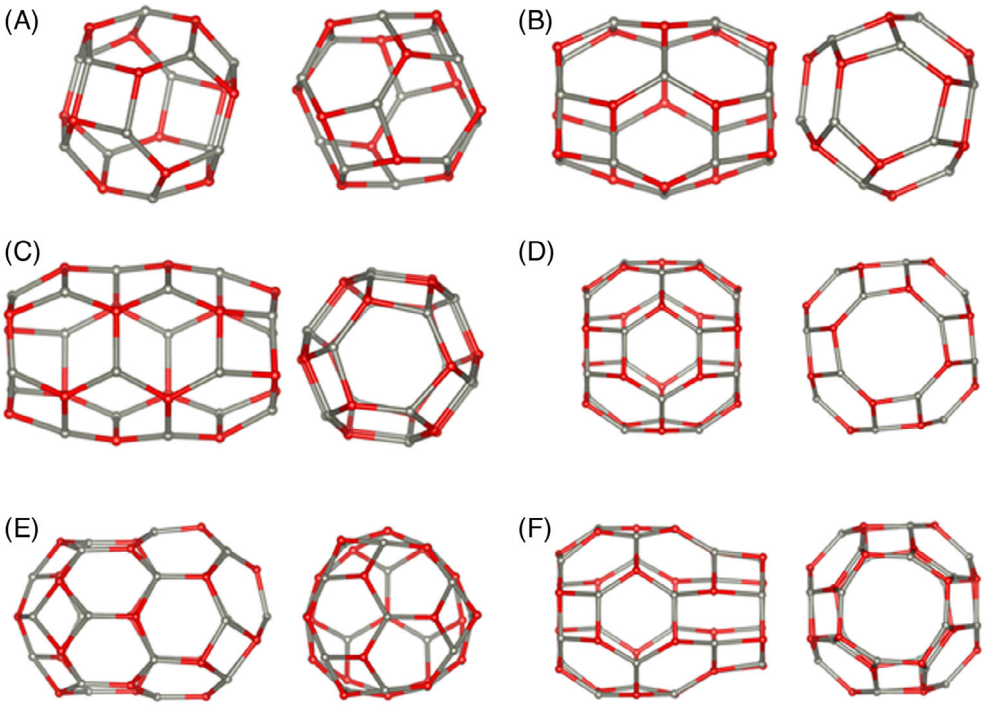

FIGURE 2 The optimized structures of pure (A) $Zn_{12}O_{12}$, (B) $Zn_{15}O_{15}$, (C) $Zn_{18}O_{18}$, (D) $Zn_{20}O_{20}$, (E) $Zn_{22}O_{22}$, and (F) $Zn_{24}O_{24}$ using B3LYP/6-311G (d,p) level of theory

TABLE 1 The calculated electronic and reactivity parameters of pure ZnO

Pure	PG	DM	E_b	HOMO	LUMO	E_g	VIP	VEA	η	μ	ω
$Zn_{12}O_{12}$	T_h	0.00	3.99	−5.96	−2.09	3.87	7.56	0.73	1.94	−4.03	4.19
$Zn_{15}O_{15}$	C_{3h}	0.00	4.04	−5.72	−2.10	3.62	7.21	0.84	1.81	−3.91	4.22
$Zn_{18}O_{18}$	S_6	0.00	4.08	−5.62	−2.10	3.52	6.90	0.93	1.76	−3.86	4.23
$Zn_{20}O_{20}$	C_{4h}	0.00	4.10	−5.66	−2.24	3.42	7.07	1.10	1.71	−3.95	4.56
$Zn_{22}O_{22}$	C_3	0.72	4.11	−5.41	−2.30	3.11	6.67	1.19	1.56	−3.86	4.78
$Zn_{24}O_{24}$	C_4	0.68	4.14	−5.43	−2.21	3.22	6.62	1.15	1.61	−3.82	4.53

Note: All values are described in eV.

absorption spectra of CH_4 and CO_2 gases adsorbed upon ZnO NCs based on CAM-B3LYP/TD-DFT method.[32–34]

3 | RESULTS AND DISCUSSIONS

The adsorption of one gas of CH_4 and CO_2 on $Zn_{12}O_{12}$, $Zn_{15}O_{15}$, $Zn_{18}O_{18}$, $Zn_{20}O_{20}$, $Zn_{22}O_{22}$, and $Zn_{24}O_{24}$ NCs were investigated in this study. In order to model the adsorption of both gases on ZnO NCs, the reactive sites of other complexes were addressed by considering molecular electrostatic potential (ESP). The ESP pertains to the electron density and is generally used to recognize sensitive areas to electrophilic and nucleophilic reactions.[35] For example, Figure 1 shows the ESP of CO_2, CH_4, and $Zn_{12}O_{12}$. Here, the negative areas (red color) and positive areas (blue color) of ESP are pertains to electrophilic and nucleophilic attacks, respectively. In order to determine the effect, the position of gases near the ZnO NCs, three to five configurations were examined for each adsorption configuration, then the most stable configurations were reported in this study.

The optimized geometries of pure $Zn_{12}O_{12}$, $Zn_{15}O_{15}$, $Zn_{18}O_{18}$, $Zn_{20}O_{20}$, $Zn_{22}O_{22}$, and $Zn_{24}O_{24}$ NCs are presented in Figure 2. Moreover, the point group (PG), dipole moment (DM), binding energy per atom (E_b), HOMO–LUMO energy gap (E_g), vertical ionization potential (VIP), vertical electron affinity (VEA), hardness (η), chemical potential (μ), and electrophilic index (ω) of all the NCs are tabulated in Table 1. Notably, the $Zn_{12}O_{12}$ NC with T_h point group (PG) is found to possess high stability in terms of small ZnO NC,[36] indicating that it is essential to use as a building block for constructing ZnO with multiform morphologies.[37] Besides, the PG of $Zn_{15}O_{15}$, $Zn_{18}O_{18}$, $Zn_{20}O_{20}$, $Zn_{22}O_{22}$, and $Zn_{24}O_{24}$ NCs are C_{3h}, S_6, C_{4h}, C_3, and C_4, respectively.

The DM in a structure is a physical factor that is essentially used to evaluate the intermolecular interactions, for example, higher dipole moment means stronger interaction.[38] The DM of the ZnO NCs shifts from 0 (for $Zn_{12}O_{12}$, $Zn_{15}O_{15}$, $Zn_{18}O_{18}$, and $Zn_{20}O_{20}$) to 0.72 Debye ($Zn_{22}O_{22}$) and 0.68 Debye ($Zn_{24}O_{24}$), depending on the increase in the size. The $Zn_{22}O_{22}$ and $Zn_{24}O_{24}$ NCs are considerably polar, which can indicate their solubility in aqueous medium, while the other NCs are nonpolar. These results indicate that increase in the size of the NCs also enhances the chemical reactivity.

The binding energy per atom (E_b) of pure ZnO NCs and adsorption energy (E_{ad}) of calculated geometries of the CH_4 and CO_2 gases adsorbed ZnO NCs are presented in Figure 3. Depending on increase in size, the E_b of the ZnO NCs increased smoothly from 3.99 to 4.14 eV, indicating the higher stability of larger ZnO NCs.

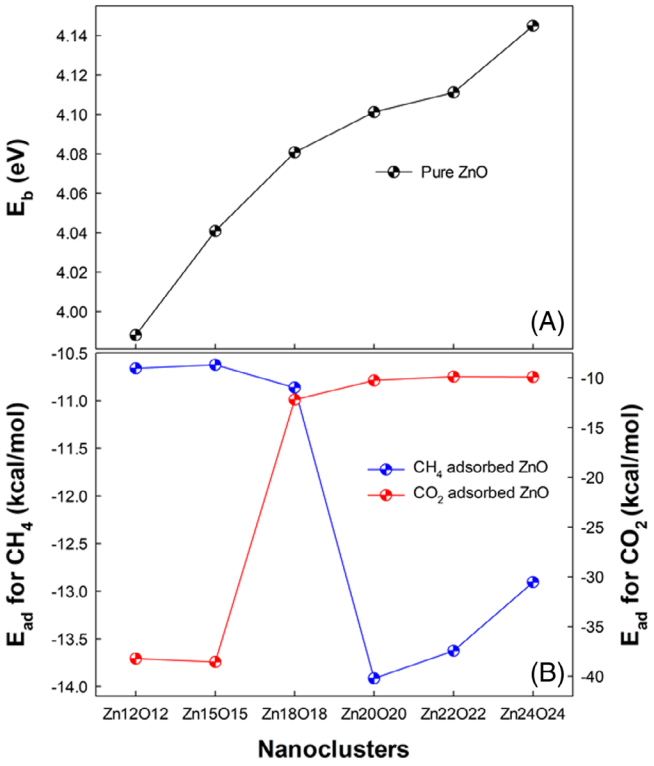

FIGURE 3 (A) Binding energies per atom (E_b) of pure (A) $Zn_{12}O_{12}$, $Zn_{15}O_{15}$, $Zn_{18}O_{18}$, $Zn_{20}O_{20}$, $Zn_{22}O_{22}$, and $Zn_{24}O_{24}$ (B) adsorption energies (E_{ad}) after the CH_4 and CO_2 adsorption

Figures 4 and 5 show the optimized geometries of CH_4 adsorption on ZnO NCs. The E_{ad} of the ZnO NCs are calculated in the range of −10.62 and −13.91 kcal/mol (for CH_4) and −9.92 and −38.24 kcal/mol (for CO_2). Since the E_{ad} is negative, there are an attractive interaction between the ZnO NCs and gases. Notably, the size of ZnO NCs has an important impact on the E_{ad} between the ZnO NCs and CH_4 and CO_2 gases. In addition, the E_{ad} (−13.91 kcal/mol) for interaction between $Zn_{20}O_{20}$ NC and CH_4 is more desirable than the other interactions $Zn_{12}O_{12}$ (−10.66 kcal/mol), $Zn_{15}O_{15}$ (−10.62 kcal/mol), $Zn_{18}O_{18}$ (−10.86 kcal/mol), $Zn_{22}O_{22}$ (−13.63 kcal/

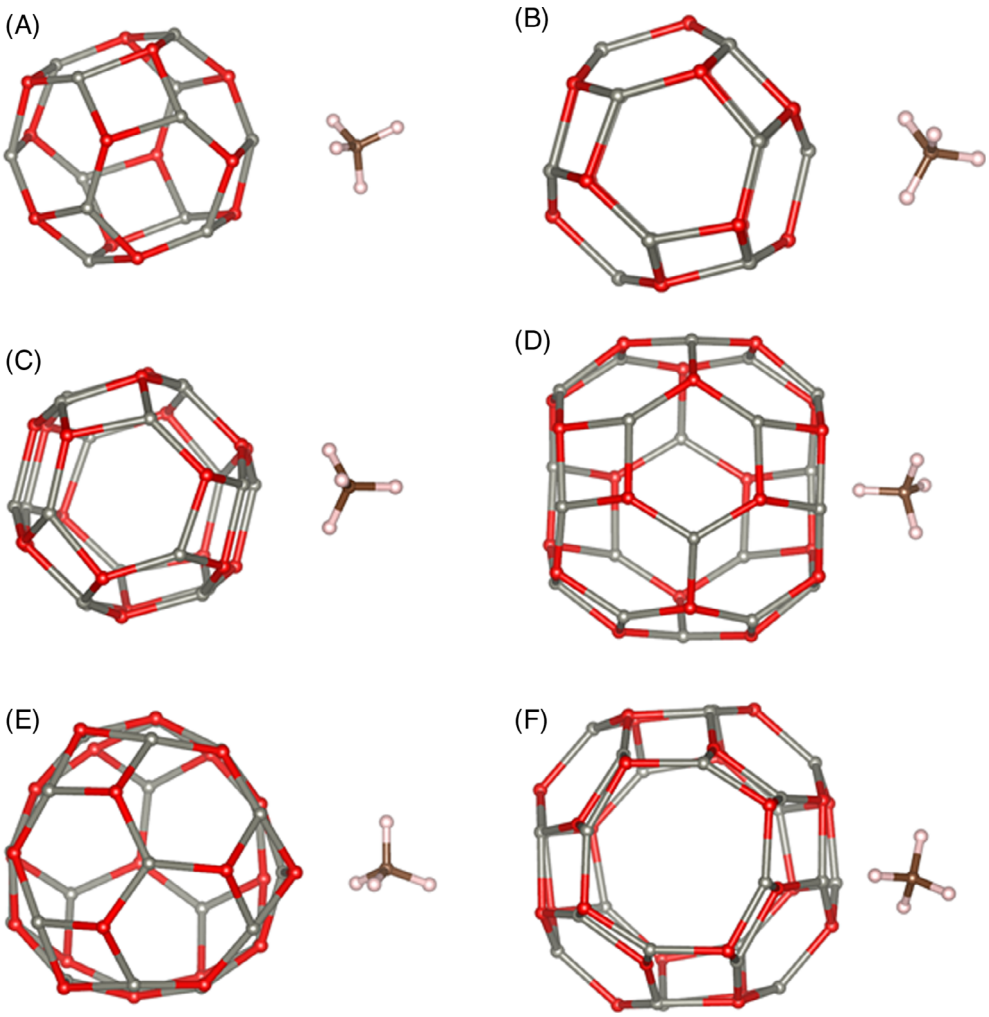

FIGURE 4 Relaxed structures of CH_4 adsorption on (A) $Zn_{12}O_{12}$, (B) $Zn_{15}O_{15}$, (C) $Zn_{18}O_{18}$, (D) $Zn_{20}O_{20}$, (E) $Zn_{22}O_{22}$, and (F) $Zn_{24}O_{24}$ using B3LYP/6-311G(d,p) level of theory

mol), and $Zn_{24}O_{24}$ (−12.90 kcal/mol), which means that the CH_4 gas can be physically adsorbed at the surface of ZnO NCs (see Figure 4 and Table 2). It is important that the increase in the size of the NCs also enhances the CH_4 adsorption. When it comes to interactions between ZnO NCs and CO_2 gas, the increase in the size of the NCs also decreases the CO_2 adsorption (Table 3). The E_{ad} of CO_2 for the most stable formation on the $Zn_{12}O_{12}$ and $Zn_{15}O_{15}$ NCs is about −38.24 kcal/mol (for $Zn_{12}O_{12}$) and −38.58 kcal/mol (for $Zn_{15}O_{15}$), which is reason via the chemisorption of CO_2. Moreover, the DM values calculated for the $Zn_{12}O_{12}$ and $Zn_{15}O_{15}$ after CO_2 adsorption are higher than the others (see Table 3). This also supports the conclusion that the interactions are chemisorption. However, the adsorption capacity decreased as the size of NCs increases and hence the CO_2 gas is adsorbed by physical adsorption (see Figure 5). Besides, the interaction between $Zn_{18}O_{18}$ NC and CO_2 is more powerful than the others. Consequently, the CH_4 gas can be both physically and chemically adsorbed as detected by the ZnO NCs.

On the other hand, the electronic behaviors were analyzed for all NCs to gain more information about these interactions and examine their sensor properties. Figures 6 and 7 show the HOMO–LUMO energy gap (E_g) and density of state (DOS) spectrums, which allow us to evaluate their electrical conductivities, for adsorptions of CH_4 and CO_2 gases on pure ZnO CNs. In this study, the percentage of difference of the E_g after the CH_4 and CO_2 adsorptions, ΔE_g values, were also calculated. As can be seen from Figure 6, the E_g generally decreases with the enlarging size of ZnO and lie in the range of 3.87–3.11 eV. The HOMO and LUMO values are found to be about −5.41 and −2.30 eV, respectively, and corresponding the E_g is found as 3.11 eV for $Zn_{22}O_{22}$ NC and the CH_4 and CO_2 interactions which are the smallest value among all NCs. Therefore, the ΔE_g value of $Zn_{22}O_{22}$ NC after adsorption of gases is higher than the others (see Figure 6) Also, the $Zn_{22}O_{22}$ NC is higher chemical reactivity than the others. When it comes to interactions between ZnO NCs and CH_4 and CO_2 gases, there was no change in the E_g and ΔE_g orders depending on the size of the ZnO NCs after adsorption. Therefore, an increase the size of ZnO NCs has no effect on CH_4 and CO_2 adsorptions. However, the E_g of $Zn_{12}O_{12}$ NC decreased slightly after CO_2 adsorption. Besides, the DOS results for $Zn_{12}O_{12}$ and $Zn_{15}O_{15}$ NCs show a deeper shift both the HOMO and LUMO levels after CO_2 adsorption (see Figure 7). The reason for this can be the chemical adsorption of the CO_2 gas on the $Zn_{12}O_{12}$ and $Zn_{15}O_{15}$ NCs. Moreover, the $Zn_{12}O_{12}$ and $Zn_{15}O_{15}$ NCs are not useful for sensor

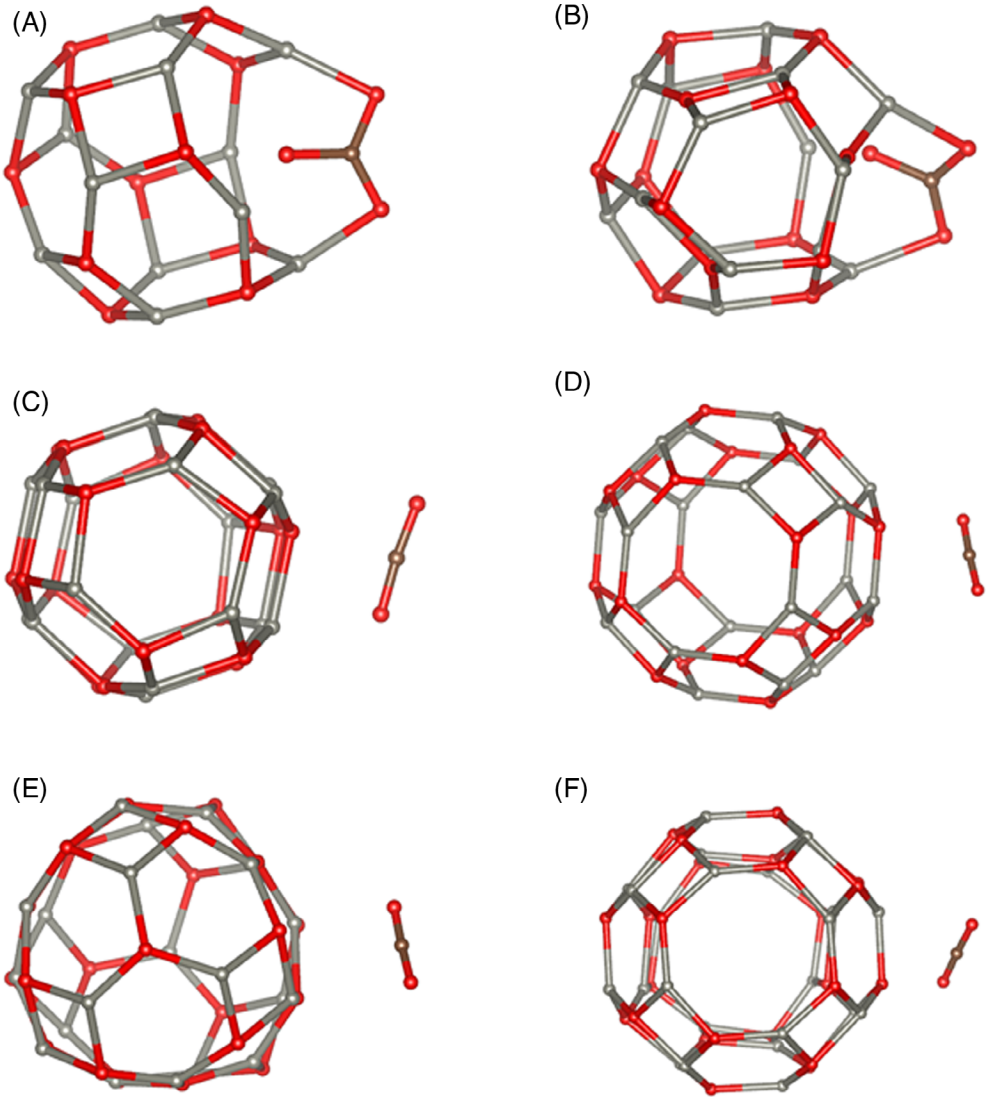

FIGURE 5 Relaxed structures of CO_2 adsorption on (A) $Zn_{12}O_{12}$, (B) $Zn_{15}O_{15}$, (C) $Zn_{18}O_{18}$, (D) $Zn_{20}O_{20}$, (E) $Zn_{22}O_{22}$, and (F) $Zn_{24}O_{24}$ using B3LYP/6-311G(d,p) level of theory

TABLE 2 The calculated electronic and reactivity parameters of ZnO complexes after the CH_4 adsorption (DM Debye, E_{ad}; kcal/mol and the others is eV)

CH_4 ads.	PG	DM	E_{ad}	HOMO	LUMO	E_g	ΔE_g	VIP	VEA	η	μ	ω
$Zn_{12}O_{12}$	C_1	0.48	−10.66	−5.94	−2.04	3.90	−0.77	7.41	0.72	1.95	−3.99	4.09
$Zn_{15}O_{15}$	C_1	0.10	−10.62	−5.75	−2.10	3.65	−0.79	7.10	0.87	1.82	−3.93	4.22
$Zn_{18}O_{18}$	C_1	0.36	−10.86	−5.63	−2.08	3.55	−0.79	6.90	0.93	1.77	−3.86	4.19
$Zn_{20}O_{20}$	C_1	0.35	−13.91	−5.67	−2.20	3.47	−1.46	6.90	1.08	1.73	−3.94	4.47
$Zn_{22}O_{22}$	C_1	0.63	−13.63	−5.44	−2.28	3.16	−1.66	6.72	1.19	1.58	−3.86	4.71
$Zn_{24}O_{24}$	C_1	0.70	−12.90	−5.46	−2.20	3.26	−1.15	6.64	1.16	1.63	−3.83	4.50

TABLE 3 The calculated electronic and reactivity parameters of ZnO complexes after the CO_2 adsorption (DM Debye, E_{ad}; kcal/mol and the others is eV)

CO_2 ads.	PG	DM	E_{ad}	HOMO	LUMO	E_g	ΔE_g	VIP	VEA	η	μ	ω
$Zn_{12}O_{12}$	C_1	4.92	−38.24	−6.07	−2.23	3.84	0.817	7.59	0.90	1.92	−4.15	4.49
$Zn_{15}O_{15}$	C_1	4.74	−38.58	−5.88	−2.21	3.68	−1.54	7.32	1.01	1.84	−4.04	4.45
$Zn_{18}O_{18}$	C_1	0.53	−12.20	−5.70	−2.13	3.57	−1.4	6.96	0.97	1.78	−3.91	4.29
$Zn_{20}O_{20}$	C_1	0.35	−10.26	−5.68	−2.23	3.45	−0.93	6.88	1.12	1.73	−3.96	4.54
$Zn_{22}O_{22}$	C_1	0.65	−9.88	−5.44	−2.28	3.16	−1.72	6.68	1.19	1.58	−3.86	4.71
$Zn_{24}O_{24}$	C_1	0.50	−9.92	−5.44	−2.20	3.24	−0.51	6.62	1.16	1.62	−3.82	4.51

applications due to chemical adsorption of CO_2 gas. The change in the electrical conductivity indicates the eventual charge-transfer interactions taking place within the complex[39] and the ΔE_g of ZnO NCs are slightly changed (0.51%–1.72%) after CH_4 and CO_2. Therefore, the studied ZnO NCs cannot pick up an electronic signal at the presence of CH_4 and CO_2 gases and cannot be employed in chemical sensors. Finally, after adsorption of CH_4 and CO_2 on ZnO NCs, it is almost impossible to design a sensor for these gases due to small changes in energy band gaps. We should also mention that the E_g values for the ZnO NCs calculated at B3LYP/6-311G(d,p) level of theory agrees perfectly with the experimental values in range of 3.2–4.6 eV.[40]

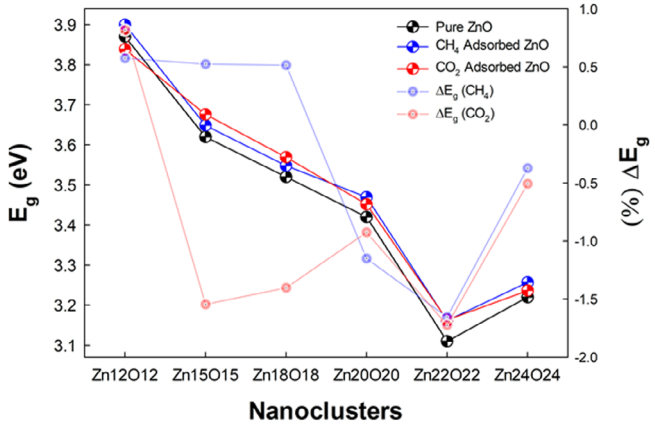

FIGURE 6 The HOMO-LUMO energy gap (E_g) and the percentage value (ΔE_g) of the difference in the E_g energies for CH_4 and CO_2 adsorptions on pure $Zn_{12}O_{12}$, $Zn_{15}O_{15}$, $Zn_{18}O_{18}$, $Zn_{20}O_{20}$, $Zn_{22}O_{22}$, and $Zn_{24}O_{24}$

The VIP and VEA of the ZnO NCs are sensitive indicators that lead to theoretical insight into the electronic structure. The VIP of the $Zn_{12}O_{12}$ NC is predicted to be 7.56 eV and has the highest value. Moreover, VIP decreases with increasing size as seen in Figure 8A. Similarly, it decreases from 7.41 to 6.64 eV (for CH_4) and 7.59 to 6.62 eV (for CO_2) after CH_4 and CO_2 adsorptions. Thus, VIP is generally found as in the following decreasing order: $Zn_{12}O_{12} > Zn_{15}O_{15} > Zn_{18}O_{18} > Zn_{20}O_{20} > Zn_{22}O_{22} > Zn_{24}O_{24}$. However, increasing the size generally enhances the VEAs of both pure and gas adsorbed ZnO NCs as seen in Figure 8B. The ZnO NC with the highest electron affinity is found as $Zn_{22}O_{22}$. Moreover, VEA is found as in the following decreasing order: $Zn_{22}O_{22} > Zn_{24}O_{24} > Zn_{20}O_{20} > Zn_{18}O_{18} > Zn_{15}O_{15} > Zn_{12}O_{12}$. These results show that as the size of ZnO NCs increases, their

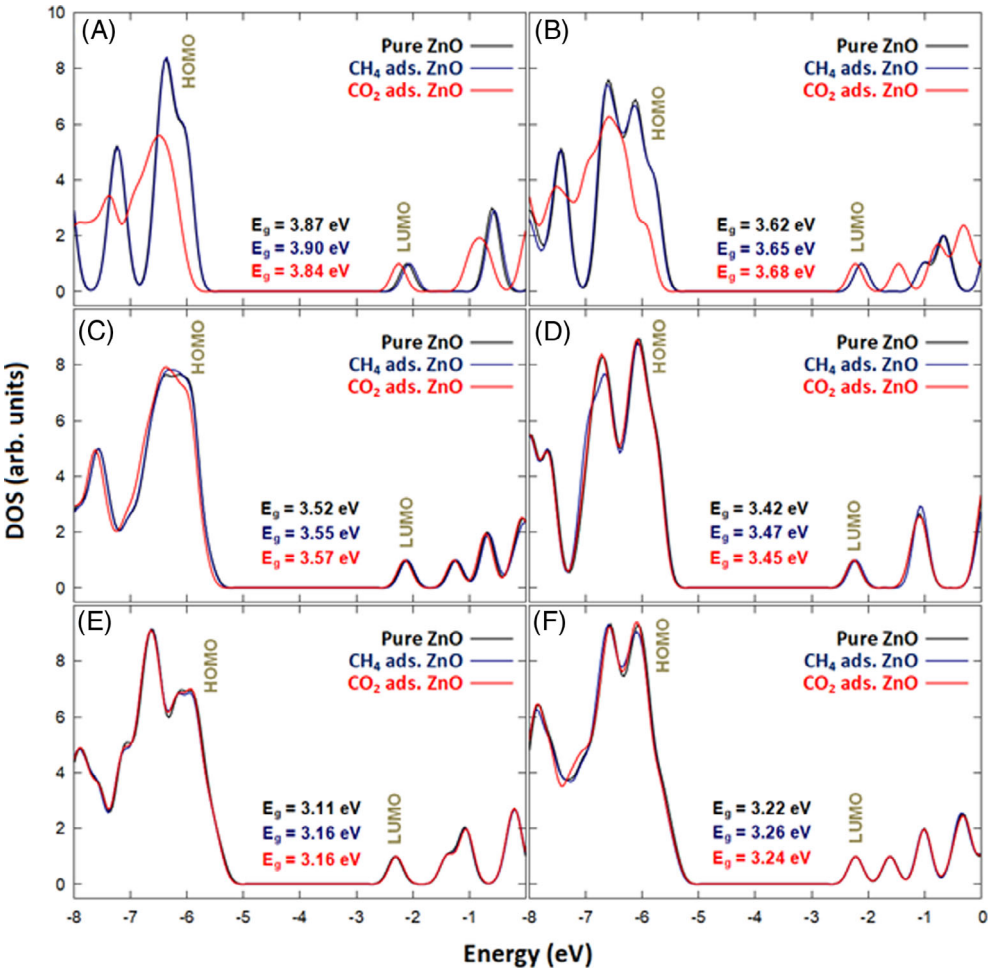

FIGURE 7 Density of states (DOS) of the CH_4 and CO_2 adsorptions on pure (A) $Zn_{12}O_{12}$, (B) $Zn_{15}O_{15}$, (C) $Zn_{18}O_{18}$, (D) $Zn_{20}O_{20}$, (E) $Zn_{22}O_{22}$, and (F) $Zn_{24}O_{24}$

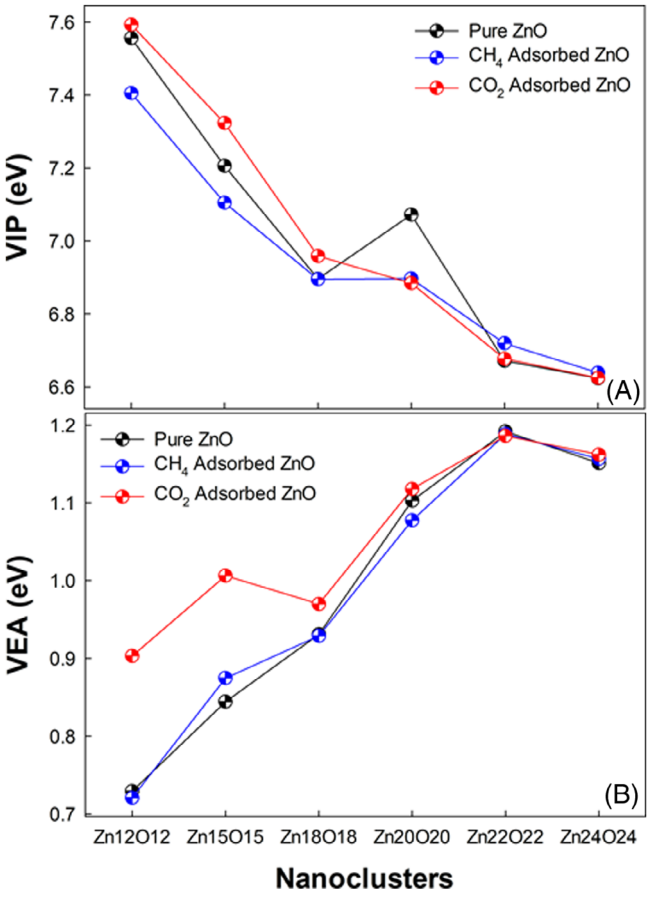

FIGURE 8 (A) VIP and (B) VEA of the CH_4 and CO_2 adsorptions on pure (A) $Zn_{12}O_{12}$, (B) $Zn_{15}O_{15}$, (C) $Zn_{18}O_{18}$, (D) $Zn_{20}O_{20}$, (E) $Zn_{22}O_{22}$, and (F) $Zn_{24}O_{24}$

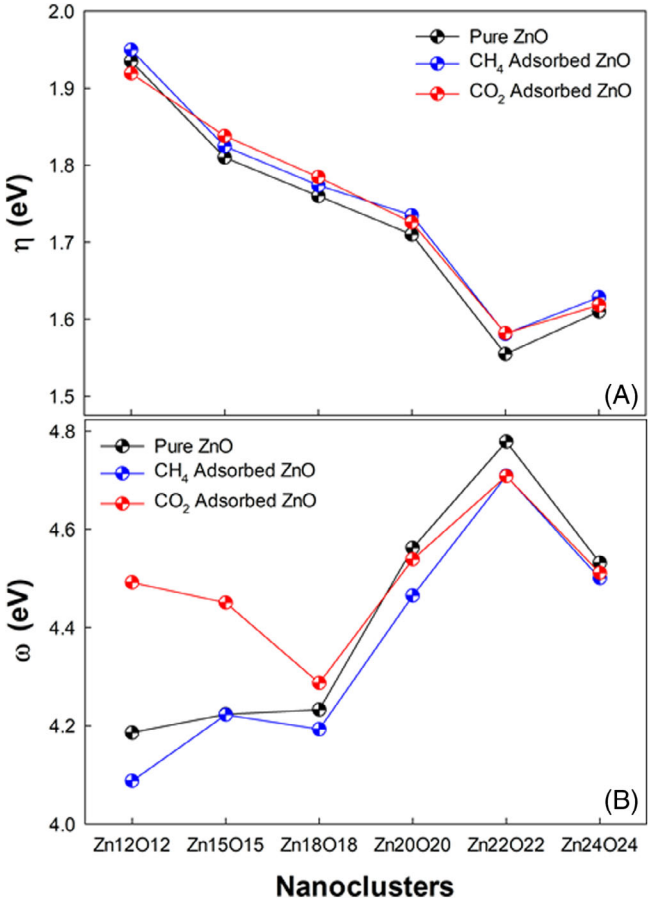

FIGURE 9 (A) η and (B) ω of the CH_4 and CO_2 adsorptions on pure (A) $Zn_{12}O_{12}$, (B) $Zn_{15}O_{15}$, (C) $Zn_{18}O_{18}$, (D) $Zn_{20}O_{20}$, (E) $Zn_{22}O_{22}$, and (F) $Zn_{24}O_{24}$

ability to lose electrons decreases and their affinity generally for electrons increases. However, the CH_4 and CO_2 adsorptions do not significantly affect the VIP and VEA trends for the ZnO NCs. The adsorption of CH_4 and CO_2 gases on ZnO NCs do not significantly affect the VIP and VEA trends. In addition, the VIP and VEA values calculated by the B3LYP/6-311G(d, p) for the ZnO NCs are in agreement with experimental data.[41,42]

In this study, chemical reactivity was examined in connection with chemical hardness (η), chemical potential (μ) and electrophilicity index (ω) (see Tables 1–3). The η decreases significantly depending on increase in the size of the ZnO NCs, but the ω increases (see Figure 9). Moreover, the η is found as in the following increasing order: $Zn_{22}O_{22} < Zn_{24}O_{24} < Zn_{20}O_{20} < Zn_{18}O_{18} < Zn_{15}O_{15} < Zn_{12}O_{12}$. Due to the chemical adsorption of CO_2 gas on $Zn_{12}O_{12}$ and $Zn_{15}O_{15}$ NCs, they have a higher ω than pure and CH_4 adsorbed NCs. However, increasing the size of the NCs or adsorption did not cause a significant change in ω. Besides, the $Zn_{22}O_{22}$ NC has the lowest η and highest ω among ZnO NCs. Increasing the size of ZnO NCs provides lower resistance to change in electronic configuration. It is worth noting that the $Zn_{22}O_{22}$ has higher chemical reactivity than other ZnO NCs.

Figure 10 shows the UV–vis absorption spectra for CH_4 and CO_2 adsorptions on the surface of ZnO NCs calculated using TD-DFT method. Depending on the increase in the size, the UV–vis absorption spectra values are generally increased and lie in the range of 274.0–291.6 nm but decreased after CH_4 and CO_2 adsorptions (see Figure 10). The UV–vis spectra of pure $Zn_{12}O_{12}$ and $Zn_{15}O_{15}$ NCs show one peak at 274 nm which belongs to the UV-C light (far UV). Besides, the maximum UV–vis spectra of the $Zn_{12}O_{12}$ and $Zn_{15}O_{15}$ NCs with adsorption are calculated about 264.4 nm (for $Zn_{12}O_{12}$) and 249.2 nm (for $Zn_{15}O_{15}$), which are reason via the chemisorption of CO_2. Depending on the increase in the size, the maximum UV–vis spectra of the $Zn_{18}O_{18}$, $Zn_{20}O_{20}$ and $Zn_{24}O_{24}$ NCs give one peak at 274.8, 278.8, and 271.6 nm, respectively. Besides, the largest shift in the UV–vis spectra is found for $Zn_{22}O_{22}$ NC, which moves from 291.6 to 286.8 nm (for CH_4) and 288.4 nm (for CO_2) after adsorption. In this study, the UV–vis spectra values calculated at B3LYP/6-311G(d,p) level of theory agree well with the experimental values obtained for ZnO NPs annealed at 200°C temperature in the range of 270–380 nm.[40,43,44] Besides, we note that the TD-DFT method is reliable to estimate UV–vis absorption spectra in the gas phase.

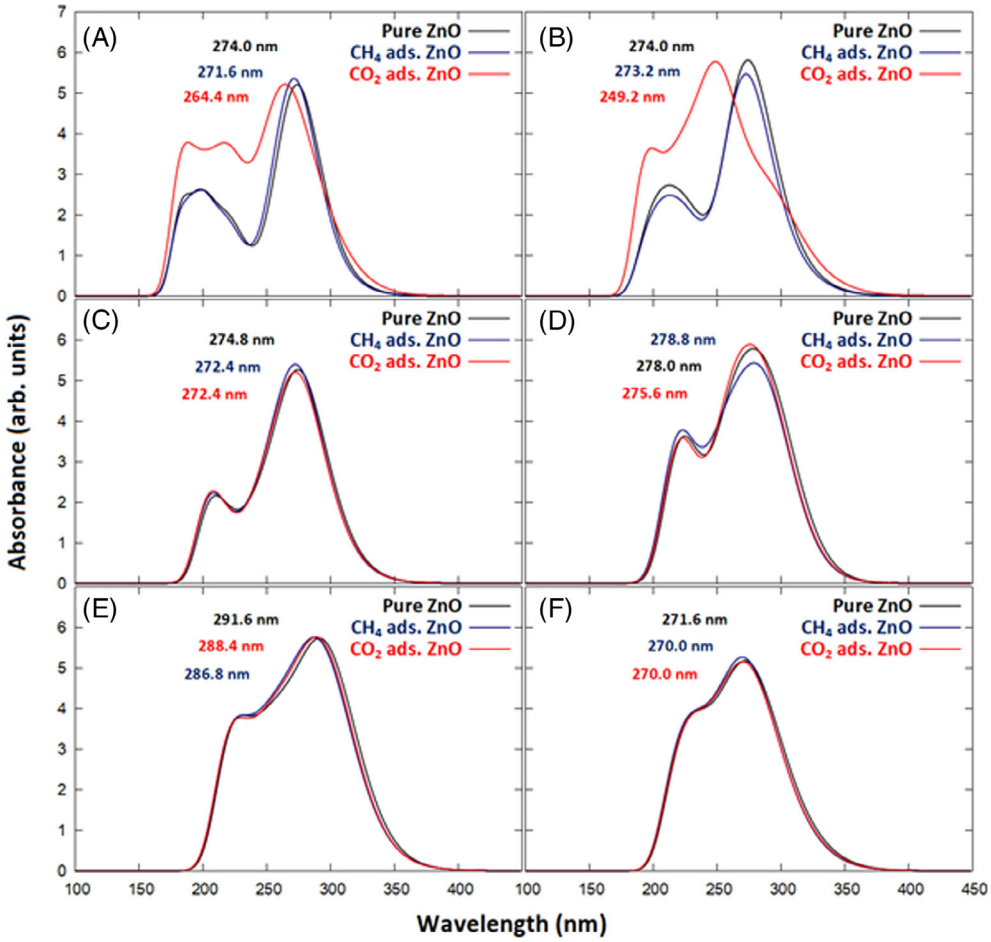

FIGURE 10 UV–vis spectra of the CH_4 and CO_2 adsorptions on (A) $Zn_{12}O_{12}$, (B) $Zn_{15}O_{15}$, (C) $Zn_{18}O_{18}$, (D) $Zn_{20}O_{20}$, (E) $Zn_{22}O_{22}$, and (F) $Zn_{24}O_{24}$

4 | CONCLUSIONS

We have initiated a theoretical investigation into the detection of CH_4 and CO_2 gases by the $Zn_{12}O_{12}$, $Zn_{15}O_{15}$, $Zn_{18}O_{18}$, $Zn_{20}O_{20}$, $Zn_{22}O_{22}$, and $Zn_{24}O_{24}$ CNs based on the framework of DFT calculations. Adsorption energy, HOMO–LUMO energy gap, the density of state, and UV–vis absorption spectra as well as chemical hardness and electrophilicity index parameters were considered to further understand the adsorption behavior of ZnO NCs in different sizes towards CH_4 and CO_2 gases. It was found that the bandgap energies of pure ZnO NCs were decreased from 3.87 to 3.11 eV, indicating the enhanced electrical conductivity of pure ZnO NCs with size. However, after adsorption, their electrical conductivity is decreased, indicating that they cannot produce an electronic signal. Besides, the CH_4 and CO_2 adsorption on studied ZnO NCs decreases the chemical reactivity and sensitivity. Since the changes in the ΔE_g and the UV–vis absorption spectra are a reliable benchmark for diagnosing the sensors of gases, thus our results show that it is almost impossible to use pure ZnO NCs as a sensor for CH_4 and CO_2 gases.

According to the results the UV–vis spectra, the maximum absorption peaks were predicted in the near-ultraviolet. Notable, the UV–vis spectra and band gap energies obtained from DFT calculations were compared with experimental results, and a good agreement has been found. It is worth noting that ZnO NCs could be one of the important nanomaterials that can be used as pure in future research for biomedical and sensor applications due to their bio-safe and biocompatible. We hope that this study will serve as a reference and a starting point for future researchers' study on functional ZnO NCs in gas sensing.

ACKNOWLEDGMENT

The numerical calculations reported were partially performed at TUBITAK ULAKBIM, High Performance and Grid Computing Centre (TRUBA resources), Turkey.

DATA AVAILABILITY STATEMENT

The data that support the findings of this study are available from the corresponding authors upon reasonable request.

ORCID

İskender Muz https://orcid.org/0000-0002-6882-5119
Mustafa Kurban https://orcid.org/0000-0002-7263-0234

REFERENCES

[1] R. A. Betts, O. Boucher, M. Collins, P. M. Cox, P. D. Falloon, N. Gedney, D. L. Hemming, C. Huntingford, C. D. Jones, D. M. H. Sexton, M. J. Webb, *Nature* **2007**, *448*(7157), 1037.
[2] J. Meyer, *Nature* **2008**, *455*(7214), 733.

[3] R. Stuart Haszeldine, *Science (80-)* **2009**, *325*, 1647.
[4] D. W. Keith, *Science (80-)* **2009**, *325*, 1654.
[5] S. Chu, A. Majumdar, *Nature* **2012**, *488*(7411), 294.
[6] S. Ghosh, P. Ranjan, S. Ramaprabhu, R. Sarathi, *Ina. Lett.* **2018**, *34*(3), 197.
[7] J. Wager, B. Yeh, R. Hoffman, D. K.-C. O. in S. State, U, *Curr. Opin. Solid State Mater. Sci.* **2014**, *18*, 53.
[8] M. Laurenti, G. Canavese, S. Stassi, M. F.-R., U, *RSC Adv.* **2016**, *6*, 76996.
[9] J. Liu, M. V. Fernández-Serra, P. B. Allen, *Phys. Rev. B* **2016**, *93*, 081205.
[10] R. Q. Song, A. W. Xu, B. Deng, Q. Li, G. Y. Chen, *Adv. Funct. Mater.* **2007**, *17*, 296.
[11] P. Hu, Y. Liu, X. Wang, L. Fu, D. Zhu, *Chem. Commun.* **2003**, *11*, 1304.
[12] J. Zhang, L. Sun, C. Liao, C. Yan, *Chem. Commun.* **2002**, *2*, 262.
[13] S. Polarz, A. V. Orlov, F. Schüth, A.-H. Lu, S. Polarz, A. V. Orlov, F. Schüth, A.-H. Lu, *Kops.uni-konstanz.de* **2007**, *13*, 592.
[14] X. Y. Kong, Y. Ding, R. Yang, Z. L. Wang, *Science (80-)* **2004**, *303*, 1348.
[15] X. Zhong, W. Knoll, *Chem. Commun.* **2005**, 1158.
[16] İ. Muz, S. Alaei, M. Kurban, *Mater. Today Commun.* **2021**, *27*, 102252.
[17] S. P. Chang, K. J. Chen, *J. Nanomater.* **2012**, *2012*, 1.
[18] A. Kołodziejczak-Radzimska, T. Jesionowski, *Materials* **2014**, *7*, 2833.
[19] R. Bai, M. Yang, G. Hu, L. Xu, X. Hu, Z. Li, S. Wang, W. Dai, M. Fan, *Carbon NY* **2015**, *81*, 465.
[20] S. Kumar, S. K. Saxena, *Mater. Renew. Sustain. Energy* **2014**, *3*, 1.
[21] A. D. Becke, *J. Chem. Phys.* **1993**, *98*, 1372.
[22] M. J. Frisch, G. W. Trucks, H. B. Schlegel, G. E. Scuseria, M. A. Robb, J. R. Cheeseman, G. Scalmani, V. Barone, B. Mennucci, G. A. Petersson, H. Nakatsuji, M. Caricato, X. Li, H. P. Hratchian, A. F. Izmaylov, J. Bloino, G. Zheng, J. L. Sonnenberg, M. Hada, M. Ehara, K. Toyota, R. Fukuda, J. Hasegawa, M. Ishida, T. Nakajima, Y. Honda, O. Kitao, H. Nakai, T. Vreven, J. A. Montgomery, J. E. Peralta, F. Ogliaro, M. Bearpark, J. J. Heyd, E. Brothers, K. N. Kudin, V. N. Staroverov, R. Kobayashi, J. Normand, K. Raghavachari, A. Rendell, J. C. Burant, S. S. Iyengar, J. Tomasi, M. Cossi, N. Rega, J. M. Millam, M. Klene, J. E. Knox, J. B. Cross, V. Bakken, C. Adamo, J. Jaramillo, R. Gomperts, R. E. Stratmann, O. Yazyev, A. J. Austin, R. Cammi, C. Pomelli, J. W. Ochterski, R. L. Martin, K. Morokuma, V. G. Zakrzewski, G. A. Voth, P. Salvador, J. J. Dannenberg, S. Dapprich, A. D. Daniels, Farkas, J. B. Foresman, J. V Ortiz, J. Cioslowski, D. J. Fox, *Gaussian 09, Revision E.01*, **2009**.
[23] W. Humphrey, A. Dalke, K. Schulten, *J. Mol. Graph.* **1996**, *14*, 33.
[24] N. M. O'Boyle, A. L. Tenderholt, K. M. Langner, *J. Comput. Chem.* **2008**, *29*, 839.
[25] R. G. Parr, R. G. Pearson, *J. Am. Chem. Soc.* **1983**, *105*, 7512.
[26] T. Koopmans, *Physica* **1934**, *1*, 104.
[27] T. Yanai, D. P. Tew, N. C. Handy, *Chem. Phys. Lett.* **2004**, *393*, 51.
[28] I. Muz, M. Kurban, M. Dalkilic, *J. Comput. Electron.* **2020**, *19*, 895.
[29] İ. Muz, F. Göktaş, M. Kurban, *Theor. Chem. Acc.* **2020**, *139*, 1.
[30] I. Muz, M. Kurban, *J. Electron. Mater.* **2020**, *49*, 3282.
[31] İ. Muz, *Mater. Today Commun.* **2022**, *31*, 103798.
[32] B. M. Wong, T. H. Hsieh, *J. Chem. Theory Comput.* **2010**, *6*, 3704.
[33] L. Xu, A. Kumar, B. M. Wong, *J. Comput. Chem.* **2018**, *39*, 2350.
[34] M. B. Oviedo, N. V. Ilawe, B. M. Wong, *J. Chem. Theory Comput.* **2016**, *12*, 3593.
[35] P. Politzer, D. Truhlar, in *Chemical Applications of Atomic and Molecular Electrostatic Potentials: Reactivity, Structure, Scattering, and Energetics of Organic, Inorganic, and Biological* (Eds: P. Politzer, D. Truhlar), Springer Science & Business Media, Springer, Boston, MA **2013**.
[36] J. M. Matxain, J. M. Mercero, J. E. Fowler, J. M. Ugalde, *J. Am. Chem. Soc.* **2003**, *125*, 9494.
[37] D. Stradi, F. Illas, S. T. Bromley, *Phys. Rev. Lett.* **2010**, *105*, 045901.
[38] J. Mawwa, S. Ud Daula Shamim, S. Khanom, M. Kamal Hossain, F. Ahmed, 2021.
[39] M. Zaboli, H. Raissi, *Struct. Chem.* **2015**, *26*, 1059.
[40] R. N. Aljawfi, M. J. Alam, F. Rahman, S. Ahmad, A. Shahee, S. Kumar, *Arab. J. Chem.* **2020**, *13*, 2207.
[41] D. E. Clemmer, N. F. Dalleska, P. B. Armentrout, *J. Chem. Phys.* **1998**, *95*, 7263.
[42] C. A. Fancher, H. L. De Clercq, O. C. Thomas, D. W. Robinson, K. H. Bowen, *J. Chem. Phys.* **1998**, *109*, 8426.
[43] P. Mitra, D. Dutta, S. Das, T. Basu, A. Pramanik, A. Patra, *ACS Omega* **2018**, *3*, 7962.
[44] Z. L. Wang, *Mater. Today* **2004**, *7*, 26.

How to cite this article: İ. Muz, M. Kurban, *J. Comput. Chem.* **2022**, *43*(27), 1839. https://doi.org/10.1002/jcc.26986